RNA (2000), *6*:1432–1444. Cambridge University Press. Printed in the USA.

Crystal structure combined with genetic analysis of the *Thermus thermophilus* ribosome recycling factor shows that a flexible hinge may act as a functional switch

TOMOHIKO TOYODA,[1] OULIANA F. TIN,[2] KOICHI ITO,[1] TOSHINOBU FUJIWARA,[1] TAKASHI KUMASAKA,[3] MASAKI YAMAMOTO,[3] MARIA B. GARBER,[2] and YOSHIKAZU NAKAMURA[1]

[1]Department of Tumor Biology, The Institute of Medical Science, The University of Tokyo, P.O. Takanawa, Tokyo 108-8639, Japan
[2]Institute of Protein Research, Russian Academy of Science, Pushchino, Moscow Region, Russia
[3]RIKEN Harima Institute, Mikazuki, Sayo, Hyogo 679-5148, Japan

ABSTRACT

Ribosome recycling factor (RRF), in concert with elongation factor EF-G, is required for disassembly of the posttermination complex of the ribosome after release of polypeptides. The crystal structure of *Thermus thermophilus* RRF was determined at 2.6 Å resolution. It is a tRNA-like L-shaped molecule consisting of two domains: a long three-helix bundle (domain 1) and a three-layer *βlαlβ* sandwich (domain 2). Although the individual domain structures are similar to those of *Thermotoga maritima* RRF (Selmer et al., *Science*, 1999, *286*:2349–2352), the interdomain angle differs by 33° in two molecules, suggesting that the hinge between two domains is potentially flexible and responsive to different conditions of crystal packing. The hinge connects hydrophobic junctions of domains 1 and 2. The structure-based genetic analysis revealed the strong correlation between the hinge flexibility and the in vivo function of RRF. First, altering the hinge flexibility by making alanine or serine substitutions for large-size residues conserved at the hinge loop and nearby in domain 1 frequently gave rise to gain of function except a Pro residue conserved at the hinge loop. Second, the hinge defect resulting from a too relaxed hinge structure can be compensated for by secondary alterations in domain 1 that seem to increase the hydrophobic contact between domain 1 and the hinge loop. These results show that the hinge flexibility is vital for the function of RRF and that the steric interaction between the hinge loop and domains 1 and 2 restricts the interdomain angle and/or the hinge flexibility. These results indicate that RRF possesses an architectural difference from tRNA regardless of a resemblance to tRNA shape: RRF has a "gooseneck" elbow, whereas the tRNA elbow is rigid, and the direction of flex of RRF and tRNA is at a nearly right angle to each other. Moreover, surface electrostatic potentials of the two RRF proteins are dissimilar and do not mimic the surface potential of tRNA or EF-G. These properties will add a new insight into RRF, suggesting that RRF is more than a simple tRNA mimic.

Keywords: gooseneck model; hinge variability; ribosome recycling factor; RRF crystallography; tRNA mimic

INTRODUCTION

After release of nascent polypeptides by polypeptide release factors (RF; RF1 and RF2), the posttermination complex composed of the ribosome, deacylated tRNA, and mRNA needs to be dissociated for the next round of protein synthesis. It is likely that the ribosomal P-site and A-site remain occupied with a deacylated tRNA and RF1 or RF2 protein (for a review, see Nakamura et al., 1996, 2000) upon release of the polypeptide chain. Early studies done by Kaji and colleagues in the 1970s showed that an extraribosomal protein, referred to as ribosome recycling factor (RRF), is required for the dissociation of the posttermination ribosomal complex in bacteria (Hirashima & Kaji, 1972). They noticed that RRF, in concert with the elongation factor EF-G, triggers a dissociation of the polysome complex into monosomes in vitro (for a review, see Janosi et al., 1996). These findings led many researchers to speculate that dissociation releases deacylated

Reprint requests to: Yoshikazu Nakamura, Department of Tumor Biology, The Institute of Medical Science, The University of Tokyo, P.O. Takanawa, Tokyo 108-8639, Japan; e-mail: nak@ims.u-tokyo.ac.jp.

tRNA and RF as a final step for recycling. Alternatively after ribosome dissociation, a translocase may be required to move deacylated tRNA and RF to the E- and P-sites of the ribosome, respectively, prior to the complete decomposition. How RRF dissociates the posttermination complex has long been puzzling.

Ehrenberg and colleagues have reported that bacterial RF3 accelerates the dissociation of RF1 and RF2 from the ribosome in a GTP-dependent manner, thereby taking part in the RF-recycling step. Rapid recycling of ribosomes requires both RF3 and RRF in vitro (Freistroffer et al., 1997; Pavlov et al., 1997). An increased RF3 activity enhanced peptide release in vivo at strong RF1- and RF2-binding signals such as UAAU and UGAU, more effectively than at the weak termination signals such as UGAC (Crawford et al., 1999). Faster rates of association of RF1 and RF2 lead to a slower rate of RF dissociation from the ribosome at strong stop signals (Poole et al., 1995), unless RF3 efficiently accelerates release of RF1 and RF2 (Crawford et al., 1999). Upon GTP hydrolysis, RF3 is also released from the ribosome, thereby leaving behind the posttermination complex with mRNA, deacylated tRNA in the P-site, and the empty A-site, which is believed to be a substrate for RRF in concert with EF-G (Hirashima & Kaji, 1972). The early work by Kaji and colleagues argued for complete decomposition of the ribosome complex into monosome, deacylated tRNA and mRNA by RRF (for a review, see Janosi et al., 1996), whereas more recent work by Ehrenberg and colleagues has argued for the release of the 50S subunit from the complex, leaving mRNA and deacylated tRNA bound to the 30S subunit in the in vitro minigene translation (Karimi et al., 1999).

While this work was being prepared for publication, the work of Selmer et al. (1999) on the structure of *Thermotoga maritima* RRF (tmRRF) was published, which provides a fascinating scenario for this puzzle. They have found that the 2.55 Å crystal structure of tmRRF superimposes almost perfectly with $tRNA^{Phe}$ except for the amino acid-binding 3′ end. They proposed that RRF was a perfect tRNA mimic to explain the mechanistic disassembly of the posttermination ribosomal complex (Selmer et al., 1999; for a review, see also Nissen et al., 2000). They speculate that RRF binds to the A-site of the ribosome and that EF-G translocates RRF from A- to P-site and deacylated tRNA from P- to E-site of the ribosome in GTP-dependent manner, where it would dissociate rapidly.

It is known that RRF is essential for bacterial growth (Janosi et al., 1998; Fujiwara et al., 1999). Recognition of a stop codon by RF is a slow process (Yarus & Curran, 1992), and it is possible that a relatively high fraction of the ribosomes are bound to the stop codon. Once these peptides are released by RF, rapid recycling of ribosomes may be important for rapidly growing bacteria. To date, RRF homologs are found universally in prokaryotes as well as in a mitochondria of the budding yeast, *Saccharomyces cerevisiae*, and chloroplasts of spinach (Rolland et al., 1999).

We have previously isolated and characterized the gene for *Thermus thermophilus* RRF (ttRRF) (Fujiwara et al., 1999). Intact ttRRF failed to complement a conditionally lethal RRF mutation of *Escherichia coli*; however, deletion of the C-terminal five amino acids of ttRRF permits complementation, suggesting a modulator activity for the C-terminal tail of ttRRF. The central architecture and functional role of RRF in translational control and the unique modulator activity of the C-terminus piqued our interest in a structural investigation. Here we present the 2.6 Å crystal structure of ttRRF. The tertiary structures of each domain of tmRRF and ttRRF are similar. There is, however, a marked difference in the hinge angle between two domains in *T. maritima* and *T. thermophilus*. We have introduced mutations into this hinge and neighboring residues of ttRRF to examine the functional importance of the hinge. Based on the genetic data as well as the structural and architectural similarities and distinctions between these two RRF proteins and tRNA, we will discuss to what extent a predicted tRNA mimic may or may not explain RRF, to get a new insight into ribosome recycling factor.

RESULTS

Crystallographic structure determination

For the structure solution of ttRRF, a conventional heavy atom search was performed, yielding a platinum derivative (Table 1). Using a single crystal of the Pt derivative, we collected diffraction data at three wavelengths ($\lambda_1 = 1.0200$ Å, $\lambda_2 = 1.07125$ Å, $\lambda_3 = 1.07176$ Å) located at fluorescence edge (two data sets) and at a distant shorter wavelength. From this data, we calculated phases using the multiwavelength anomalous dispersion (MAD) methodology (Table 1; see Materials and Methods for details). The final model included all 185 amino acids, and 84 water oxygens. The final R and R_{free} values were 23.2% and 30.5%, respectively (Table 1), with a mean positional error of 0.38 Å (Luzzati, 1952).

With a molecular mass of 20,994 Da, RRF is one of the smallest translational factors. The portion of ttRRF defined by the electron density has dimensions of $60 \times 45 \times 25$ Å and consists of two domains (Fig. 1A). The topological scheme of secondary structures is given in Figure 1B. Domain 1 is a three-helix bundle containing residues 1–29 and 107–185. Helices H1 (residues 3–26), H4 (residues 108–146), and H5 (residues 151–183) are tightly packed against each other with extended hydrophobic interaction. Domain 2 is a globular structure containing residues 34–102, in which four-stranded antiparallel β-sheet (S3, S4, S6, and S5) on one side and two-stranded antiparallel β-sheet (S1 and

TABLE 1. Crystallographic data collection and statistics of the final model of ttRRF.

	Native	Pt λ_1	Pt λ_2	Pt λ_3
Space group	$P3_221$		$P3_221$	
Cell constant a (Å)	71.5		71.5	
Cell constant c (Å)	79.6		79.5	
Wavelength (Å)	1.5418	1.0200	1.07125	1.07176
Resolution (Å)	50–2.6	50–2.2	50–2.2	50–2.2
(last shell)	(2.66–2.6)	(2.25–2.2)	(2.25–2.2)	(2.25–2.2)
Completeness (%)	99.7	97.8	98.1	98.1
(last shell)	(98.7)	(93.5)	(93.1)	(94.3)
$\langle I \rangle / \langle \delta I \rangle$	17.6	24.3	22.9	23.4
Multiplicity	3.8	3.0	3.0	3.0
R_{merge}	0.038	0.038	0.038	0.038
(last shell)	(0.234)	(0.209)	(0.241)	(0.231)
Phasing power[a]				
Centric		—	1.00	1.06
Acentric		—	1.78	1.73
R_{cullis}[a]				
Centric		—	0.72	0.73
Acentric		—	0.71	0.70
Anomalous		0.86	0.84	0.85
Figure of merit		0.51	(50–3.0 Å resolution)	
After solvent flattening		0.73	(50–3.0 Å resolution)	
Refinement				
Resolution (Å)	10–2.6			
R factor	0.232			
R_{free}	0.305			
Number of water molecules	84			
Average B-factors (Å^2)				
Main chain	50.2			
Side chain	55.3			
Rmsd bonds	0.013			
Rmsd angles	1.93			
Ramachandran plot (%)				
Most favored	92.9			
Disallowed	0.0			

[a]The reference wavelength for phasing purposes was λ_1.

S2) and two short α helices (H2 and H3) on the other side are positional to point their hydrophobic side chains to the interior. Thus, domain 2 exhibits a sandwich enveloping an extended hydrophobic core, which stabilizes the domain structure. Domains 1 and 2 are bridged by two loops, loop 1 (residues 30–33) and loop 2 (residues 103–106). The contact area of the domains is 892 Å^2 (7.6%) out of the total area of the two domains. This is lower than normal and is interpreted as indicating that the interaction between domains 1 and 2 is relatively weak.

Comparison to *T. maritima* RRF

The primary structures of ttRRF and tmRRF proteins are 43% identical without any internal gaps or inserts (Fig. 2). Their secondary structures are almost identical except that a four-residue α helix is assigned between S2 and S3 β-strands in tmRRF (Selmer et al., 1999), but is missing in ttRRF. Hence, helices H4 and H5 of ttRRF correspond to H5 and H6 of tmRRF. Each domain structure of ttRRF superimposes almost perfectly with tmRRF (Fig. 3). Root mean square derivative value of distance between two Cα chains upon fitting is approximately 1.4 Å in domain 1 and 1.6 Å in domain 2. However, their overall structures are remarkably distinct because two domains of ttRRF and tmRRF are oriented differently. When two crystal structures are compared on the basis of one domain, the other domain rotates 33° between two molecules (see Fig. 3).

The hinge structure

Domains 1 and 2 are bridged by loop 1 and loop 2, which we refer to as a hinge. These two loops are composed of conservative residues in different RRF proteins (see Fig. 2). Because there is no strong interaction between domains 1 and 2 of ttRRF and tmRRF, the hinge may be potentially flexible and the different interdomain angles of both crystals may be reflecting the different packing conditions suitable for individual crystal growth. Comparison of the two RRF structures

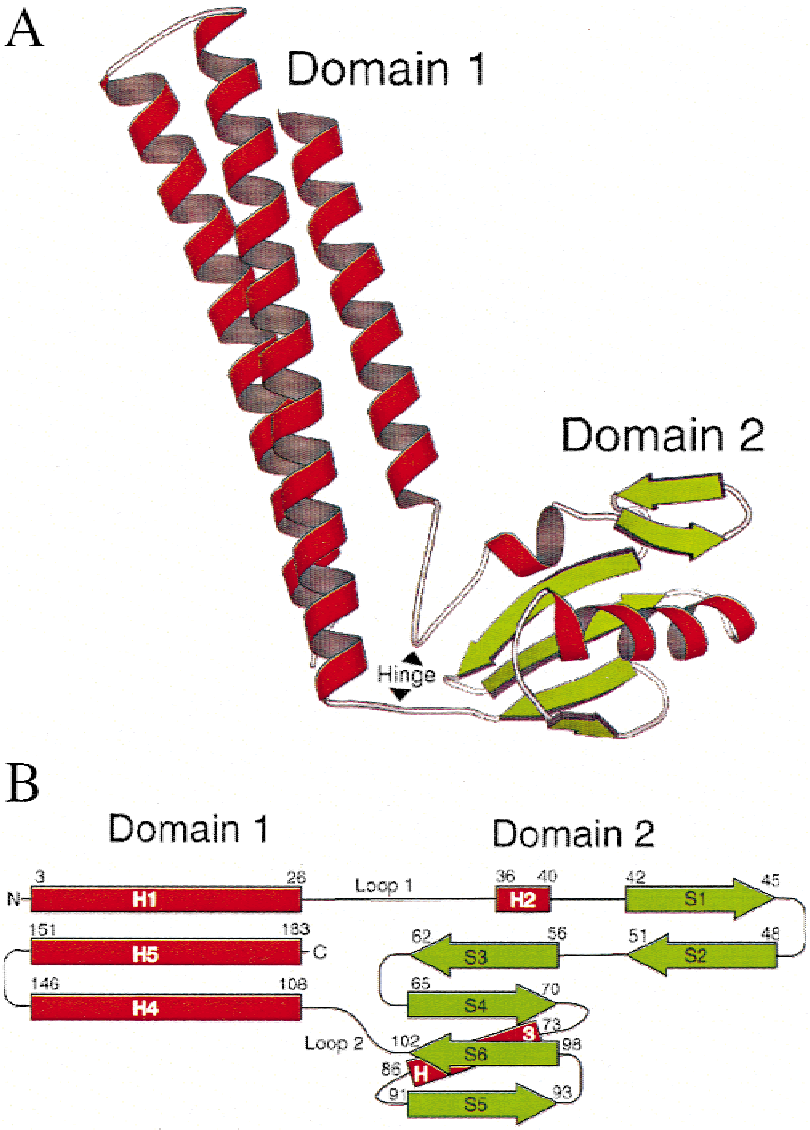

FIGURE 1. Schematic drawings of the structure of ttRRF. **A:** Ribbon diagram of ttRRF showing the overall fold. α-helices and β-strands are drawn in red and green, respectively. **B:** Topology diagram of ttRRF. Color coding is the same as in **A**.

suggests that the movement of the hinge may be favored to rotate around the axis crossing the two loops (Fig. 4A, shown as a blue bar). This speculation gets some support from the structural point of view. First, both termini of loop 2 are part of the hydrophobic cores of two domains (see below), hence the flexibility of loop 2 may be restricted by the remaining two residues including Pro. Second, loop 1 and loop 2 are weakly, if at all, connected by hydrophobic interaction between the main chain of loop 1 and the side chain of loop 2, forming a friable surface, as seen also with tmRRF. Therefore, the hinge is likely to prefer a rotation around the axis on this surface although the movement to other direction(s) could not be excluded completely at present. We will refer to this flexibility as a "gooseneck" model.

Functional assessment of hinge loop 2

Hydrophobic amino acids are conserved in loop 2 (positions 103–106) and Pro is universally conserved at position 104 (see Fig. 2). To investigate the functional importance of the hinge structure, we substituted Ala individually for Ile, Pro, Pro, and Leu at positions 103–106 of ttRRF, and examined the activity of these variants by the intergeneric complementation test using the temperature-sensitive lethal RRF mutant of *E. coli* (*frr-3*). It is known that the intact ttRRF is unable to complement the *E. coli frr-3* mutation (Fujiwara et al., 1999). However, Ala substitutions for Ile103 and Leu106 conferred the ability to complement for full-length ttRRF, resulting in a gain-of-function phenotype. Specifically, *E. coli frr-3* cells transformed with ttRRF-bearing plasmids containing either an I103A or L106A allele grew almost normally at 42 °C, whereas Ala variants for Pro104 and Pro105 grew poorly under these conditions (Table 2). These results suggest potentially distinct roles for the central two Pros and the flanking Ile and Leu for the action of RRF in heterologous conditions. It is conceivable that the flexibility of the hinge is increased by reducing the size of residues 103 and

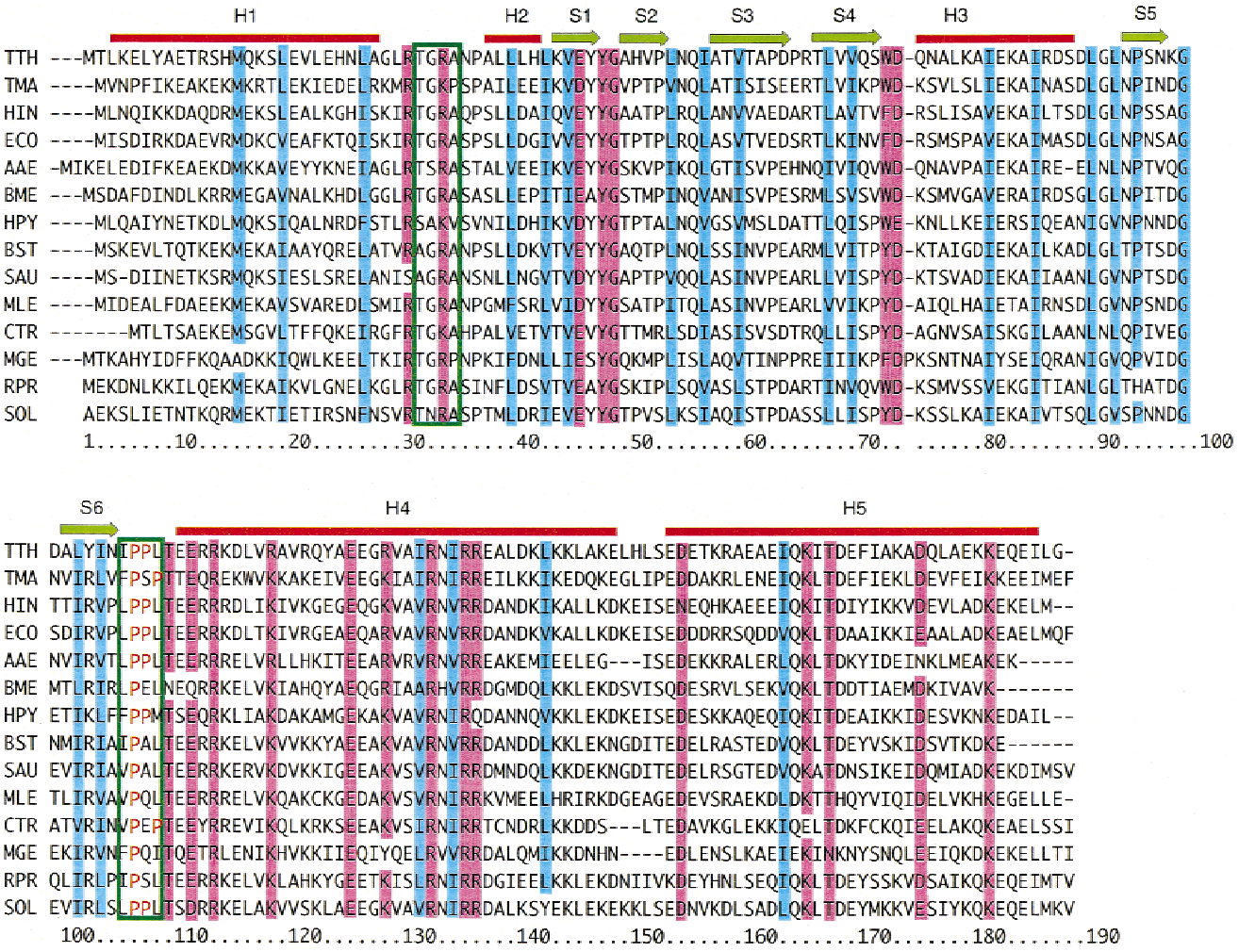

FIGURE 2. Alignment of representative RRF sequences from different bacteria. The species aberrations are given as follows: TTH, *Thermus thermophilus* (GenBank accession number AB016498); TMA, *Thermotoga maritima* (AE001792); HIN, *Haemophilus influenzae* (P44307); ECO, *Escherichia coli* (P16174); AAE, *Aquifex aeolicus* (AE000703); BME, *Brucella melitensis* (U53133); HPY, *Helicobacter pylori* (P56398); BST, *Bacillus subtilis* (Z99112); SAU, *Staphylococcus aureus* (AF033018); MLE, *Mycobacterium leprae* (Z97369); CTR, *Chlamydia trachomatis* (U60196); MGE, *Mycoplasma genitalium* (P47673); RPR, *Rickettsia prowazekii* (Q9ZE08); SOL, *Spinacia oleracea* (AJ133751). The numbering corresponds to ttRRF. Red rectangles and green arrows indicate α-helices and β-strands, respectively. Conserved or conservatively substituted residues in the molecular surface are colored pink, hydrophobic core residues are colored blue, and the hinge residues are marked by green boxes.

106, which are directly connected to hydrophobic cores of both domains (discussed below), leading to gain of function, whereas Pro is architecturally required for restricting the hinge orientation (see Fig. 5A).

Functional assessment of hinge loop 1

Loop 1 of the hinge is composed of conserved residues, most of which are small hydrophilic amino acids such as Thr, Gly, and Ala at first, second, and fourth positions, except for Arg32 at the third position (see Fig. 2). Given that the size of amino acids in the hinge loop may influence the activity of RRF, one could speculate that the conserved Arg32 residue might play a critical role as well. To test this assumption, Arg32 was replaced by Ser, Ala, or Gly, and the resulting variants were examined for their complementation capacity. As shown in Table 2 with the intact C terminus, Ser, Ala, and Gly variants acquired complementation activity, with the efficiency of complementation related to the size of the substitution: the smaller the side chain, the better the gain of function.

Functional assessment of C-terminal tail

To assess what role the C-terminal residues have, we removed amino acids one by one from the C terminus (EKKEQEILG at positions 177–185) of ttRRF, and monitored complementation activity in the *E. coli* RRF mutant. Removing one, two, or three amino acids did not

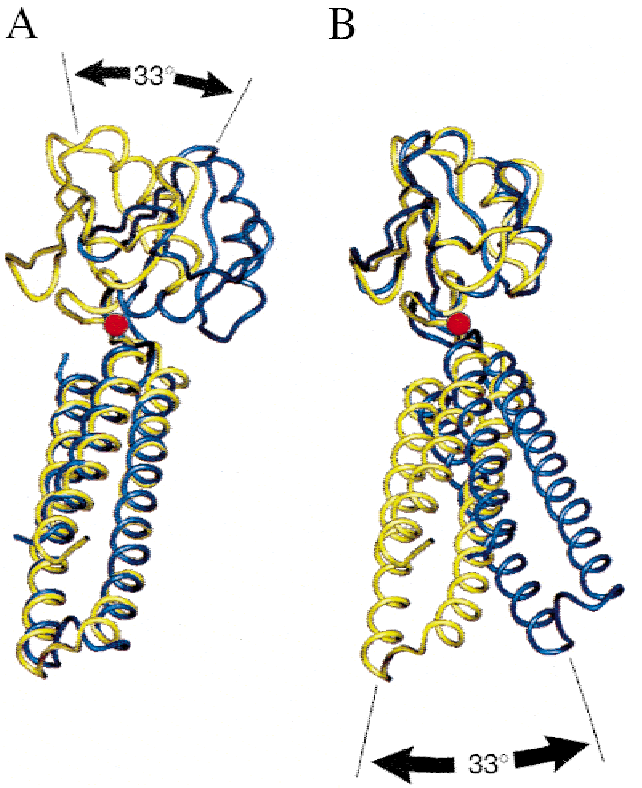

FIGURE 3. Ribbon diagram representation of the superposition of ttRRF (yellow) and tmRRF (blue; Protein Data Bank accession code 1dd5) viewed down the rotation axes (marked by red dots) of molecules. **A:** Domain 1 is superimposed. **B:** Domain 2 is superimposed. Note that each domain is nearly identical between ttRRF and tmRRF but rotates 33°.

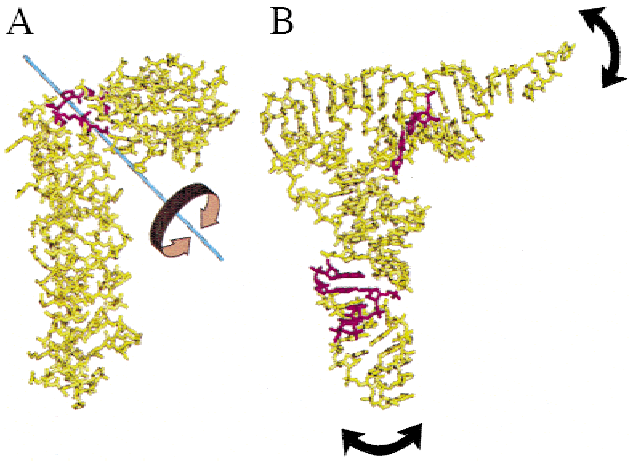

FIGURE 4. Comparison of molecular mobility between ttRRF and $tRNA^{Phe}$. **A:** ttRRF. **B:** Yeast $tRNA^{Phe}$. Hinge regions are colored purple: residues 30–33 and 103–106 of RRF (this article), and nt 7, 28–30, 42, 43, and 66 of tRNA (Matsumoto et al., 1999). A rod penetrating RRF is the rotation axis of the molecule. Arrows indicate the direction of movement of each rigid group.

confer any detectable activity, but removal of Glu182 in the variant with four amino acids deleted exerted a small but significant capacity to complement the *E. coli* defect. As expected, deletion through Gln181 (referred to as ΔC5) conferred on ttRRF the full capacity to compensate for the *E. coli* RRF defect. This gain-of-function property of ttRRF was retained with deletions up to eight amino acids, but was abolished upon removal of the ninth amino acid. These results confirmed that the C-terminal tail, especially the edge of α helix H5, plays a critical role in modulating the RRF activity.

A string of charged residues constitutes positions 177–182 (EKKEQE). These charged amino acids cluster at the helical region close to loop 2 and may decrease the flexibility required for the action of ttRRF with the *E. coli* translational apparatus. The removal of these residues may eliminate steric hindrance and increase the flexibility of the hinge variability, leading to a gain of function. To test this assumption, serial bulky-to-small amino acid substitutions were generated for Glu182 to Glu177, corresponding to the set of serial deletions created above. These substitutions should not affect the α helical configuration. Surface residues, Lys178, Gln181, and Glu182, were substituted to Ser, and interior residues, Lys179 and Glu180, were substituted to Ala. Consistent with the prediction, Glu182 → Ser enabled ttRRF to compensate fully for the *E. coli* RRF defect (Table 2). These results suggest that a steric (or electrostatic) hindrance between the hinge and the C-terminal tail restricts the activity of ttRRF. Other serial variants, KKESS, KKASS, KAASS, SAASS, and KAEQS (where substitutions are underlined), more or less acquired the

TABLE 2. Intergeneric complementation activity of *T. thermophilus* RRF variants carrying mutations in the hinge and C-terminus.

	Complementation capacity with C-terminal change		
Hinge mutation	Intact (…KKEQEILG)	ΔC5 (…KKE)	Glu182 → Ser (…KKEQSILG)
None (wild type)	+/−	+++	+++
Experiment 1 (loop 1 mutagenesis)			
R32S	+	ND	ND
R32A	++	ND	ND
R32G	+++	ND	ND
Experiment 2 (loop 2 mutagenesis)			
I103A	++	+/−	++
P104A	+/−	+/−	++
P105A	+/−	++	ND
L106A	+++	+	+++

Mutations in hinge loop 1 (experiment 1) and loop 2 (experiment 2) were manipulated by site-directed PCR mutagenesis in *T. thermophilus* RRF protein carrying intact, ΔC5, and Glu182 → Ser C-termini. Plasmid pIQV27 derivatives carrying these singly or doubly altered ttRRF genes were transformed into temperature-sensitive lethal *frr-3* strain (YN3576), and transformant cells were streaked on LB agar plate and incubated at restrictive temperatures above 39 °C. Intergeneric complementation capacity was scored by colony size and growth: +++: normal growth (large colony); ++: fair growth (medium colony); +: weak growth (small colony); +/−, sick growth (tiny colony); −, no growth. ND: no data.

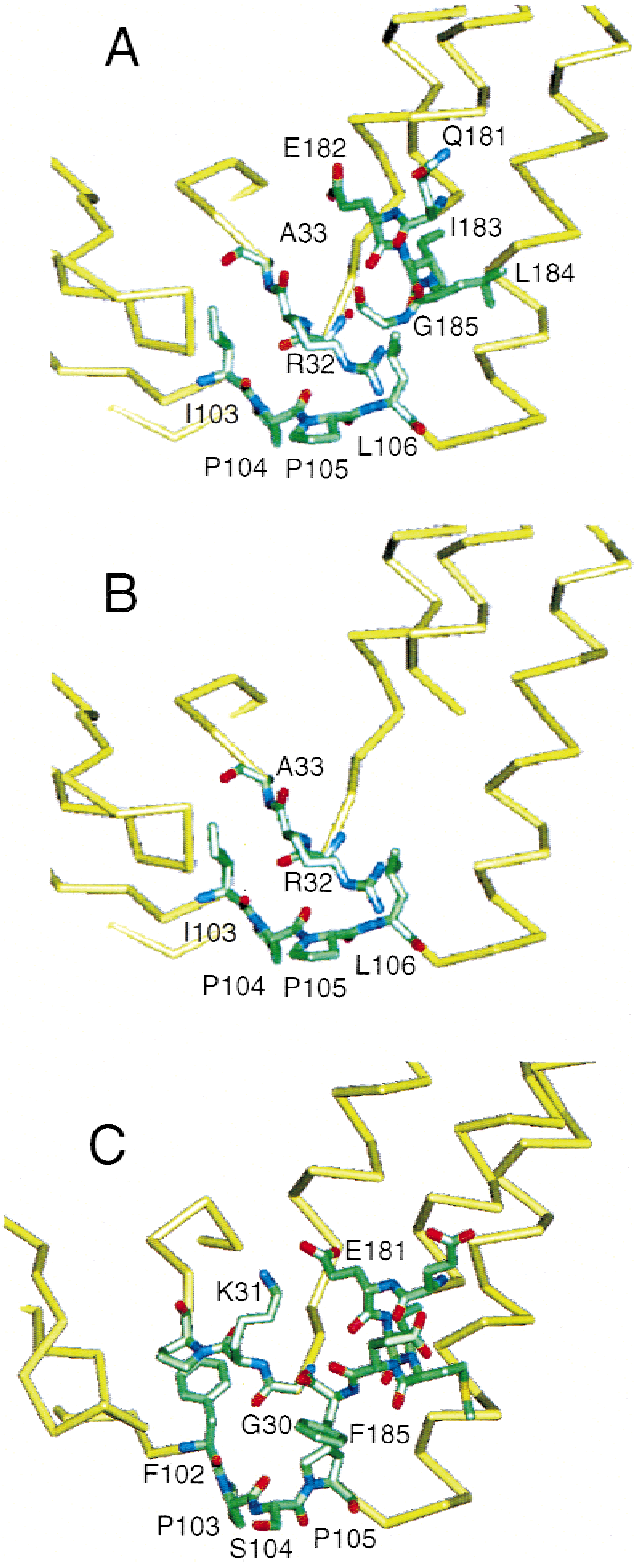

FIGURE 5. Three-dimensional structure of the hinge region. **A:** Wild-type ttRRF in which hinge loops and C-terminal 5 residues are colored green. **B:** ttRRFΔC5 (ttRRF structure from which C-terminal five residues are removed). **C:** tmRRF.

capacity to complement the *E. coli* RRF defect (data not shown) although some of these alterations might also affect the α-helical configuration.

Functional interplay between hinge and C-terminal tail

When loop 2 Ala substitutions, including gain-of-function ones, were combined with another gain-of-function change, ΔC5, these double alterations, with the exception of the Pro105 → Ala change, reduced or nullified the acquired activity of ttRRFΔC5 (Table 2, ΔC5). Therefore, the hinge alterations showed opposite effects on the RRF activity depending on whether its C-terminus was intact or truncated (see Fig. 5A,B), showing that the alterations in loop 2 and the C-terminus are not synergistic. These genetic observations suggest that the C-terminus and the hinge at loop 2 of RRF are interactive. The loop 2 Ala variants did not impair the acquired capacity of the Glu182 → Ser change (Table 2), suggesting that the presence of a complete C-terminal tail is required to maintain correct hinge flexibility in the absence of Ile103 or Leu106.

Genetic selection of compensatory alterations

Genetic selection was designed to provide compensatory alterations for loss-of-function alleles to direct our understanding of functional and/or physical intradomain and interdomain interactions. First, plasmid pIQV27 carrying the ttRRF-P104A hinge variant was mutagenized with hydroxylamine (allowing both C → T and G → A substitutions), transformed into the RRF knockout *E. coli*, and viable colonies were selected. Fourteen independent ttRRF revertants on the plasmid that acquired the complementation activity were characterized. They were grouped into three classes containing amino acid substitutions at positions 106, 180, and 182 (Table 3). Based on the steric view, the conservative Pro104 is required for curving the hinge of ttRRF; a newly borne Phe106 in the same loop 2 may substitute for this bending via compensatory hydrophobic interaction (prediction A in Table 3). The other two variations may not be directly involved in the hinge function, but may participate in the other fate of protein interaction or stability (prediction B, discussed below).

Second, intragenic suppressors were selected from ttRRFΔC5 and also carrying Pro104 → Ala using the mutator strain mutagenesis (unbiased mutagenesis). Twenty-four revertants thus isolated were classified to 11 secondary substitutions at 10 positions (Table 3). Five alleles are located in domain 1 and the other half are in domain 2 (see Fig. 7). Intriguingly, none of them overlapped with alleles obtained from a single P104A variant (discussed below). From the structural point of view, it is not immediately obvious how these suppressors are able to compensate for the defective hinge except for Val115 → Met and Ala117 → Val. Because Val115 and Ala117 are part of the hydrophobic core of α helix H4 and are located near the junction to the hinge, these small-to-bulky amino acid changes might

TABLE 3. Secondary mutations compensating for the hinge defect

Parental allele in		Suppressor	Number of isolates	Prediction of action[a]
loop 2	C-terminus			
Pro104 → Ala	intact	Leu106 → Phe	2	A
		Glu180 → Lys	1	B
		Glu182 → Lys	11	B
Pro104 → Ala	ΔC5	Glu22 → Lys	3	B
		His23 → Arg	1	B
		Glu44 → Lys	6	C
		Thr57 → Ile	5	C
		Pro61 → Ser	1	C
		Val67 → Met	1	C
		Val67 → Ala	1	C
		Asp72 → Gly	1	C
		Val115 → Met	1	A
		Ala117 → Val	1	A
		Gln120 → Arg	3	B
Ile103 → Ala	ΔC5	Ala103 → Val	8	A
		Gln120 → Arg	2	B
		Glu135 → Lys	10	B
		Glu135 → Gly	2	B

Plasmid pIQV-ttRRF carrying the indicated parental alleles was mutagenized by passing through the mutator strain XL1-Red or by treatment with hydroxylamine, and phenotypic revertants were selected at 42 °C upon transformation into the *frr-3* strain (YN3576). Plasmids that acquired the capacity to complement the *E. coli* RRF defect were analyzed by DNA sequencing.

[a]Prediction of the mode of suppression from the structural point of view: A: compensatory interdomain interaction within RRF (to increase the hydrophobic core); B: compensatory interprotein interaction with ribosomes or other translational component(s) (speculation and no experimental evidence); C: no prediction. Amino acid positions are marked in Figure 7.

strengthen the hydrophobic core and compensate for the Pro104 → Ala change (prediction A in Table 3).

Third, intragenic suppressors were also selected from ttRRFΔC5 carrying Ile103 → Ala. Of 22 revertants analyzed, 4 substitutions were assigned to positions 103, 120, and 135 (Table 3). One frequent alteration, Ala103 → Val (i.e., Ile103 → Ala → Val), is assumed to restore a more functional flexibility, instead of a friable inactive structure, of the hinge by replacing a hydrophobic large-mass residue at position 103, which probably gives rise to increased interaction with the hydrophobic core of domain 1. Perhaps the other three substitutions may restore the activity by influencing the interaction between RRF and the ribosome or other translation factors, or restore protein stability (prediction B in Table 3, discussed below).

Structural comparison to tRNA

Liljas and colleagues have reported an almost perfect mimic of the tRNA shape by tmRRF (Selmer et al., 1999). The crystal structure of ttRRF confirms this proposal and further reveals several architectural differences between RRF proteins and tRNA molecules. First, although RRF (as reported in this article) and tRNA show considerable flexibility in the overall structure, their conformational flexibility is achieved at different positions (see Fig. 4). The flexible hinge is placed at the elbow of the L shape in RRF, whereas those of tRNA are placed in the aminoacyl acceptor stem (colored red) and the anticodon helix (colored red) of tRNA (Matsumoto et al., 1999). Therefore, the elbow of RRF is flexible but that of tRNA is rigid. Second, the hinge between domains 1 and 2 of RRF is variable around the rotation axis placed on the surface determined by loop 1 and loop 2 (Fig. 4A). On the other hand, the overall conformational flexibility is induced upon binding to aminoacyl-tRNA synthetases (Ruff et al., 1991) to give rise to a widened angle of the overall L shape of tRNA (Fig. 4B). Hence, the rotation axes are at a nearly right angle to each other. Third, two gooseneck configurations possessing a 33° angular difference are detectable in RRF crystals, whereas such a structural derivative of tRNA has never been detected in crystallographic or NMR analysis. Fourth, the electrostatic surface potential of ttRRF is not shared with tmRRF, and is distinct from tRNA as well as EF-G (Fig. 6). The overall electrostatic feature of ttRRF is neutral and there are no significant areas rich in negative charges on the surface, suggesting that electrostatic attraction may not play a role in binding to the A-site pocket. These properties will give us a hint as to what is necessary for the RRF activity in addition to a tRNA mimic (discussed below).

DISCUSSION

Hinge architecture and flexibility of ttRRF

The crystal structure of ttRRF solved in this study is very similar to that of tmRRF in each domain but the interdomain angle differs by 33° between the two RRF molecules. The hydrophobic interaction between the hinge, particularly terminal residues of loop 2, Ile103 and Leu106, and the junction residues of domains 1 and 2 plays a critical role for the interdomain angle and the hinge flexibility. Structural-prediction-based mutational analysis supported this view. In principle, reducing the size of amino acids at the hinge loops increased hinge flexibility, leading to gain of function of ttRRF. For instance, Ile103 → Ala and Leu106 → Ala substitutions at the junctions of loop 2 conferred intergeneric complementation activity to ttRRF. Similarly small amino acid substitutions for the bulky Arg32 residue in loop 1 also gave rise to a gain-of-function phenotype. The bulky side chain of Arg32 sticks out from loop 1 toward domain 1 (see Fig. 7), creating a steric hindrance that is reduced by reducing the size with Ser, Ala, and Gly substitutions.

Another important element that modulates the hinge flexibility is the junction of domain 1 to the hinge. It is known that, upon removal of C-terminal five amino acids,

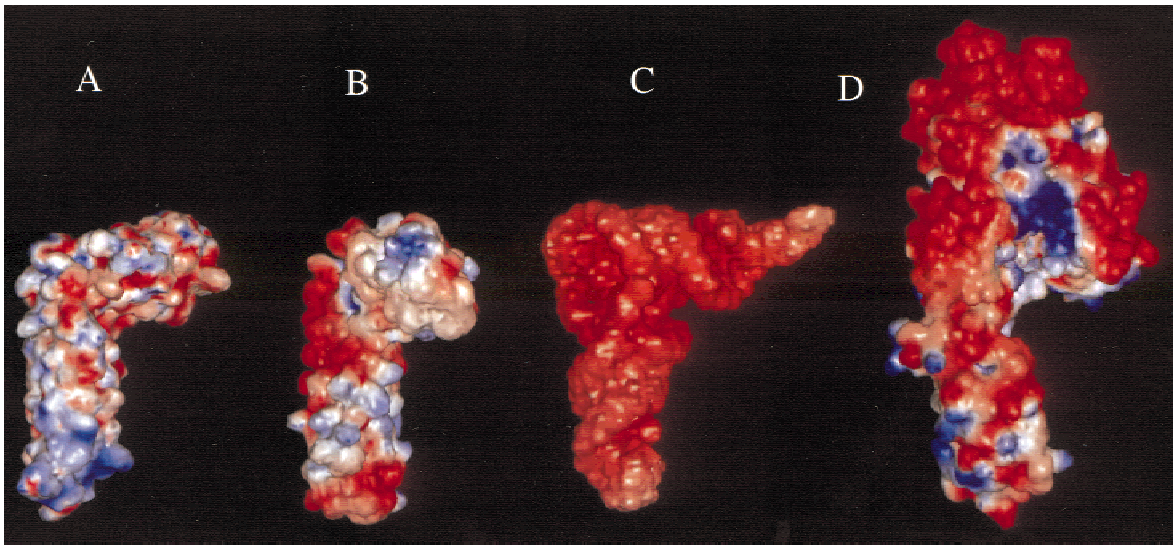

FIGURE 6. Surface electrostatic potential of ttRRF compared with those of tmRRF, $tRNA^{Phe}$, and EF-G. Positive and negative charges are colored blue and red, respectively. The potentials were calculated with the program DELPHI. **A:** ttRRF. **B:** tmRRF. **C:** Yeast $tRNA^{Phe}$. **D:** *T. thermophilus* elongation factor EF-G:GDP (Protein Data Bank accession code 1DAR).

ttRRF acquires the capacity to complement the *E. coli* RRF defect. The crystal structure of ttRRF revealed that these C-terminal amino acids are spatially integrated into α helix H5, to cause a steric contact between the hinge (colored pink) and C-terminal (colored red) atoms (Fig. 8). When the domain rotates around the axis, the steric contact between domain 2 and the C-terminal atoms restricts or modulates the flexibility. This steric hindrance may be removed by deletion of five residues (ΔC5). Reducing bulk by small amino acid substitution at the C-terminal part also supports this view. Of these residues, Glu182 protrudes out from a helix bundle (domain 1) toward domain 2 (see Fig. 7). The Glu182 → Ser replacement may remove this protrusion. The crystal structure of tmRRF suggests a salt bridge between Arg32 and Glu182. Therefore, both alterations may cause the same effect on hinge flexibility. Furthermore, ΔC5 removes Ile183 and Leu184, which are part of the hydrophobic core of domain 1, suggesting that partial loss of the hydrophobic core might contribute to the hinge flexibility through structural instability. Taking these into consideration, it is pointed out that two elements are major determinants of the hinge flex-

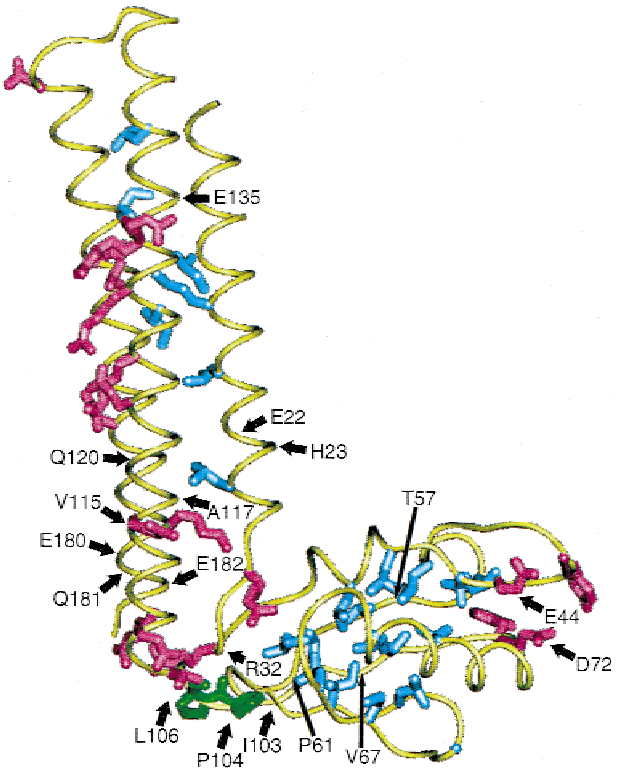

FIGURE 7. Structural distribution of conserved and conservatively substituted residues in molecular surface (pink) and in hydrophobic core (blue). Conserved prolines in hinge 2 are colored green. Positions of suppressor alleles are indicated (see Table 3).

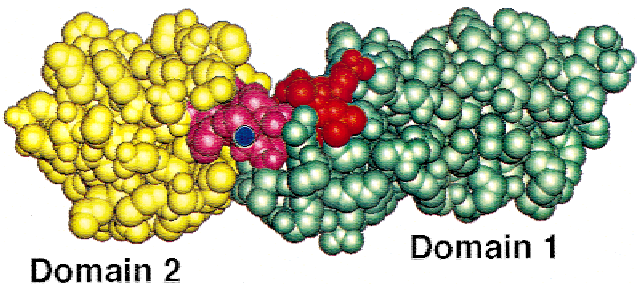

FIGURE 8. A space-filling model of ttRRF viewed down the rotation axis of the molecule. A blue circle in the molecule is the axis. Domain 1 and domain 2 are colored in green and yellow, respectively. The hinge residues are colored pink, and C-terminal five residues are colored red.

ibility: steric hindrance involving residues in loop 1 and C-terminal tail, and hydrophobic interaction involving residues in loop 2 and C-terminal tail.

Functional importance of the hinge flexibility

Multiple alignment of RRF proteins of different species highlight conservative amino acids (Fig. 2). These conservative residues of RRF are assigned to surface (colored red) or interior (colored blue) part of domains 1 and 2 (Fig. 7). Conserved surface residues may create a site for interaction with the ribosome or other translational components, whereas conserved interior residues may create a hydrophobic core for each domain. The two distinct angles found at the hinge in ttRRF and tmRRF crystals may not reflect the functional structure, but may be due to different conditions of crystal packing. If so, this also supports the idea of a flexible hinge for these thermophilic RRF molecules. Nevertheless, this flexibility is probably less than that of *E. coli* RRF because ttRRF is inactive in *E. coli* under heterologous conditions and alterations to increase its flexibility provide an active form of ttRRF. Perhaps a more rigid conformation of the hinge as compared with nonthermophilic bacteria is required at the temperature encountered in *T. thermophilus*. Although the *E. coli* RRF structure is not known, we speculate that the increased hinge flexibility caused by neighboring mutations allows the variant ttRRF to fulfill the required function in *E. coli* ribosomes. Most of the loop 2 mutants became inactive or much less active when combined with ΔC5. Perhaps the combination of the two changes creates a too relaxed hinge structure that is unable to function. This defective hinge architecture can be compensated for by secondary changes in domain 1 (helix H4) that increase sizes of hydrophobic residues, such as Val115 → Met and Ala117 → Val, at the hinge junction, leading to stabilization of a too relaxed hinge structure. These compensatory alterations suggest a change in steric positioning or contact is functionally important at the hinge. These changes are classified as group "A" in Table 3.

Other compensatory mutations were also isolated that do not seem to affect the hinge directly because their positions are remote from the hinge in the tertiary structure. One class, referred to as "B," is a frequent alteration and all class B substitutions reduce negative charge and/or increase a positive charge. Although there is no direct evidence, we assume they might influence the interplay of ttRRF with the *E. coli* ribosome. Alternatively, these positions may be important if a change from negative to positive charge at these positions helps in an indirect way to restore the active interdomain angle or hinge flexibility of the ttRRF variant, or protein stability. Domain 1 possesses 16 conservative residues on the surface, which are assigned to α helices H4 and H5 and the hinge but not to helix H1. Of the 16 residues, 10 are positive, 4 are negative, and 2 are neutral. These asymmetric distributions of negative charge residues (see Fig. 6) may play a role in binding to the ribosome or other translational component(s). The other alterations are localized in domain 2: the mechanism of suppression in these cases is not immediately predictable (class "C").

The type of compensatory mutations formed for the hinge variant, Pro104 → Ala, depend on whether the C-terminus is present or deleted. Distinct mutational types were formed for each condition (Table 3). This is not because of different mutagens used, because 6 out of 11 substitutions generated by mutator mutagenesis were C → T or G → A substitutions that are potentially inducible by hydroxylamine. Therefore, the nonoverlapping pattern of suppressors may be reflecting the structural difference of the Pro104 → Ala hinge with or without the C-terminal tail of ttRRF. All these observations strongly support the crucial importance of the interdomain angle and/or the hinge flexibility for RRF action. This is consistent with the prediction derived from the structural comparison of ttRRF and tmRRF. We feel that this natural deviation in structure created at the interface created by the two loops and two domains may provide a promising target site for developing an antibacterial compound that targets RRF. It is also noteworthy that there are several natural RRF variants that lack C-terminal residues, such as those from *Aquifex aeolicus, Brucella melitensis,* and *Bacillus subtilis* (see Fig. 2). It remains to be tested whether they complement *E. coli* RRF mutations as does a ttRRFΔC5 variant.

A tRNA mimic

Based on the superimposition of $tRNA^{Phe}$ or *T. maritima* RRF, a perfect tRNA mimic hypothesis has been proposed by Selmer et al. (1999). Their model predicts that RRF interacts with the posttermination ribosome complex in a manner similar to a tRNA, leading to disassembly of the complex. This would mean that RRF in concert with EF-G translocates the deacylated tRNA from P- to E-site, where it would dissociate rapidly. This model, however, is not consistent with biochemical findings by Karimi et al. (1999), in which deacylated tRNA remains very tightly bound to the P-site of the 30S ribosome after the action of RRF and EF-G split the ribosome into 30S and 50S subunits. Ultimately, initiation factor IF3 is strictly required for the removal of the deacylated tRNA. The counterargument from a tRNA mimic standpoint is that Karimi et al. (1999) used short mRNAs coding for not more than four amino acids and that the Shine–Dalgarno sequence of this mRNA continues to interact with 16S rRNA and impairs the postulated translocation of RRF from A- to P-site, thereby making IF3 essential. These arguments remain to be tested experimentally.

Regardless of a resemblance to tRNA shape, there are several architectural differences between tRNA and RRF as revealed in this study; the gooseneck elbow of RRF in contrast to the rigid elbow of tRNA, flex directions at right angles (see Fig. 4), or dissimilar surface electrostatic potentials (see Fig. 6). The conformational flexibility of both RRF and tRNA should be important for the action of both molecules with the ribosome or the aminoacyl-tRNA synthetase. Nevertheless, the differences in the site of flexibility and the direction of movement could be interpreted as showing that, at some stage upon binding to the ribosome, they probably act in different ways for different purposes.

If intact RRF binds to the A-site of the ribosome as argued by Selmer et al. (1999) whereas deacylated tRNA remains bound to the P-site of the 30S ribosome after dissociation of two ribosome subunits by the initial action of RRF and EF-G as argued by Karimi et al. (1999), RRF must exert its action within the A-site in concert with EF-G. EF-G can generate a post- to prepeptidyltransfer transition state of the ribosome coupled with GTP hydrolysis. It is tempting to speculate that this energy-driven transition may involve distortion of the interface between 30S and 50S ribosome particles. One plausible scenario might be that either domain connected by a flexible gooseneck of RRF may penetrate into a distorted interface and interfere with post- to prepeptidyltransfer transition, shifting the equilibrium toward a direct uncoupling of 30S and 50S. Because there are yet limited experimental data on the action of RRF in the ribosome, the mechanistic significance of a mimic of tRNA shape by RRF remains to be verified. Mapping the position of RRF in the ribosome by directed radical footprinting (Wilson & Noller, 1998) or cryoelectron microscopy (Agrawal et al., 1998) will show unambiguously the site for RRF binding in the ribosome, providing an experimental clue to understanding the biological significance of a tRNA mimic by RRF.

Molecular mimicry between protein and RNA was first suggested by Nyborg and colleagues when they saw that the crystal structure of the EF-Tu:GTP: aminoacyl-tRNA ternary complex has high structural similarity with EF-G, for example, so that domain IV of EF-G mimics the anticodon stem of tRNA (Nissen et al., 1995) (see Fig. 6). The recently published crystal structure of human eRF1 (Song et al., 2000) and tripeptide anticodon of bacterial release factors (Ito et al., 2000) revealed that release factors can mimic tRNA structurally and functionally. Selmer et al. (1999) have argued that the mimicry analogy may hold also for the recycling step of protein synthesis from the crystallographic data. A mimic of the shape of a tRNA may be an entrance pass to sit in the cockpit (A-site) in a ribosome "machine." However, the action once sitting there should be diverse for the different translation factors (reviewed by Nakamura et al., 2000). Nature must have evolved this "art" of molecular mimicry using different proteins for the diverse actions, still keeping a similar shape to fulfill the requirement of the ribosome. We assume that nature may not have created such a tRNA-mimicking protein simply to substitute for tRNA unless the protein is required to pursue some function(s) that tRNA cannot do. The genetic studies reported in this article are in line with this aim and prove useful to clarify to what extent a tRNA mimic may or may not explain RRF. This sort of structure-borne functional studies will help to understand the truth about ribosome recycling factor.

When this article was near completion, we became aware of a very recent study that warrants mention. Kim et al. (2000) have reported the crystal structure of *E. coli* RRF that is similar to ttRRF and tmRRF. Interestingly, crystallization of *E. coli* RRF required the presence of a detergent, decyl-β-D-maltopyranoside, which is packed into the hydrophobic cleft formed by several residues from domain 1, the hinge, and domain 2. Although it is not known whether the interdomain angle of *E. coli* RRF differs from the other two RRF structures or not (because the Protein Data Bank coordinate of *E. coli* RRF is not available), these authors postulated a potential domain movement around the hinge, which is consistent with the present findings.

MATERIALS AND METHODS

Protein expression and purification

The ttRRF protein was overproduced in a bacterial expression system (Fujiwara et al., 1999). *E. coli* BL21(DE3) transformed with pET30-ttRRF plasmid was grown at 37 °C to the cell density of 0.7 A_{600}. Expression of ttRRF was induced by addition of isopropyl-1-thio-β-D-galactoside (final 0.5 mM), followed by 3 h culture at 37 °C. Harvested cell paste (2 g) was suspended in 16 mL of buffer A (50 mM Tris-HCl, pH 7.0, 10 mM $MgCl_2$, 5 mM β-mercaptoethanol) containing 500 mM NH_4Cl, and sonicated. The cell debris and ribosomes were removed from the cell lysate by two successive centrifugations (16,000 $\times$ *g* for 20 min and 100,000 $\times$ *g* for 30 min). The supernatant was heated at 65 °C for 15 min and denatured *E. coli* proteins were removed by centrifugation. Crystalline ammonium sulfate was added to the cleared supernatant up to 1.5 M and the protein solution was loaded onto a Butyl-Toyopearl column (10 mL). A linear gradient of 1.5–0 M ammonium sulfate in buffer A was used for elution. Fractions containing ttRRF were combined, dialyzed against buffer A, and were further purified on a Heparin-Ultragel column (15 mL) using a linear gradient of 0–1 M NH_4Cl in buffer A. The protein was purified to near homogeneity with impurity less than 3% as judged by SDS-polyacrylamide gel electrophoresis, and concentrated to 10–15 mg/mL.

Crystallization and data collection

Crystals of the native ttRRF protein were grown at 20 °C by the hanging drop vapor diffusion technique. Three volumes of protein solution containing 10–15 mg protein/mL were mixed

with one volume of the precipitant solution: 2 M ammonium sulfate, 0.1 M Na acetate trihydrate, pH 4.6 (Crystal Screen, Hampton Research). Normally, crystals grew within two weeks to a maximal size of 0.3 × 0.3 × 0.25 mm^3. The mother liquor was replaced by cryo-solution containing 30% glycerol, and flash-frozen in a nitrogen stream at 110 K. The space group was $P3_221$ with unit cell dimensions of $a = b = 71.5$ Å, $c = 79.6$ Å, suggesting one molecule per asymmetric unit. Diffraction data of the native crystal was collected with CuKα radiation using a Rigaku R-AXIS IV imaging plate mounted on an ultraX 18 X-ray generator. Heavy-atom derivative crystals were prepared by soaking native ones in a solution containing 1 mM Na_2PtCl_4 and 1.8 M ammonium sulphate in 90 mM sodium acetate (pH 4.6). Data sets from the Pt derivative crystal were subsequently taken at 110 K at beam line BL45XU (Yamamoto et al., 1998) of the SPring-8 Synchrotron, Harima, Japan, employing a Rigaku R-AXIS IV imaging plate. Three wavelengths ($\lambda_1 = 1.0200$ Å, $\lambda_2 = 1.07125$ Å, $\lambda_3 = 1.07176$ Å, for remote, peak, and edge datasets, respectively) were chosen from the fluorescence spectrum of the crystal. All data sets were integrated using DENZO and merged using SCALEPACK (Otwinowski & Minor, 1997).

Structure determination and refinement

Platinum sites were identified by Bijvoet difference Patterson interpretation with SHELX-97 using data between 50 and 4.0 Å resolution. The refinement of heavy atom positions and calculations of MAD phases were carried out with MLPHARE (Collaborative Computational Project, Number 4, 1994) using 50–3.0 Å resolution data. These initial phases were refined by solvent flattening and histogram matching with DM (Collaborative Computational Project, Number 4, 1994). At first, solvent content was set to 50–60% of the unit cell for the calculated value of 60%. In an electron density map, three long helices (about 100 residues) were easily traced, but other parts were not observed. Then we tried solvent flattening again with lower solvent contents, 5, 10, 20, 30, and 40%, to prevent a weak electron density in the molecular region from being flattened. The best results were obtained with 20% solvent content. An initial model consisting of 130 residues was built in the electron density map using QUANTA (Moleculart Simulations Inc., San Diego). After positional refinement using X-PLOR (Brünger, 1992), model and experimental phases were combined using SIGMAA (Collaborative Computational Project, Number 4, 1994). These steps were repeated ten times until about 90% of the whole molecule were traced. In the next stage, phases were calculated from a model structure after positional refinement and were refined by solvent flattening and histogram matching with DM. A mask, calculated from the model structure (sphere radius = 4.0 Å), was used for this phase refinement and the solvent content was set to be 40% of the unit cell. These steps were repeated 24 times until the whole molecule was traced. Finally, water molecules were added to the model structure and positional and B-factor refinements were performed several times. The correctness of the model structure was confirmed by omit map. The final *R*-factor was 23.2% (R_{free} = 30.5% calculated from 5% of the data) at 2.6–10 Å resolution. Analysis using PROCHECK (Laskowski et al., 1993) showed that no residues fell outside of the allowed region of the Ramachandran plot. The final structure includes 1,478 nonhydrogen atoms and 84 water molecules. The structure coordinates have been deposited with the Protein Data Bank (http://www.rcsb.org/pdb; accession code 1EH1).

Site-directed mutagenesis

ttRRF variants were manipulated by site-directed mutagenesis using polymerase chain reaction (PCR). The loop 1 mutations were designed in sense oligonucleotides: R32A, 5′-GGGGCTCGAGGTCCTGGAGCACAACCTGGCAGGCC TCGCCACCGGCCGCGCCAACCCCG-3′; R32S, 5′-GGGG CTCGAGGTCCTGGAGCACAACCTGGCAGGCCTCTCCAC CGGCCGCGCCAACCCCG-3′; and R32G, 5′-GGGGCTCG AGGTCCTGGAGCACAACCTGGCAGGCCTCGGCACCGG CCGCGCCAACCCCG-3′. These mutation fragments amplified by PCR using these sense primers and a universal (antisense) primer, and their *Xho*I-*Bam*HI digests were ligated into the same sites of plasmid pIQV-ttRRF. The loop 2 mutations were designed in sense oligonucleotides: I103A, 5′-GGACGCGTTATACATCAACGCCCCGCCCCTCACGGA GGA-3′; P104A, 5′-GGACGCGTTATACATCAACATCGCGC CCCTCACGGAGGAAAG-3′; P105A, 5′-GGACGCGTTATA CATCAACATCCCGGCCCTCACGGAGGAAAGGCG-3′; and L106A, 5′-GGACGCGTTATACATCAACATCCCGCCCGCCA CGGAGGAAAGGCGAAAG-3′. These altered C-terminal segments were amplified by PCR using these sense primers and a universal (antisense) primer, and their *Mlu*I-*Bam*HI digests were ligated into the same sites of plasmid pIQV-ttRRF. The C-terminal ΔC5 deletion (Glu181 → amber allele) was introduced into relevant variants by substituting the *Stu*I-*Bam*HI (ΔC5) segment from ttRRF*181 (Fujiwara et al., 1999) for the wild-type segment, and tested for the activity under nonsuppressor (sup^0) conditions. The Glu182 → Ser variant was generated by replacing the wild-type *Stu*I-*Bam*HI sequence with the mutant segment amplified by PCR using a universal upstream sense primer and C-terminal antisense primer designed for the Glu182 → Ser allele (5′-GGGGATCCTCAGC CCAGGATTGACTGCTCCTTCTTCTCCGCCA-3′). The sequence of these variants was confirmed by DNA sequencing.

Suppressor selection

In vivo mutagenesis of the ttRRF gene was performed by passage through the mutator strain XL1-Red (*endA1 gyrA96 thi-1 hsdR17 supE44 relA1 lac mutD5 mutS mutT* tetracycline-resistant; Stratagene). In vitro mutagenesis was performed by incubation of plasmid DNAs with 0.4 M hydroxylamine at pH 6.0 for 20 h at 37 °C as described previously (Oshima et al. 1995; Ito et al., 1998). Complementation and suppressor selection experiments employed a conditionally lethal *frr-3* strain of *E. coli* (YN3576; Fujiwara et al., 1999), which is lethal above 39 °C. Compensatory variants were selected as survivors at 42 °C upon transformation of YN3576 with mutagenized plasmid DNAs. Plasmid DNAs were recovered, retransformed into the same parental strain, and those that gave a reproducible phenotype were further characterized. The entire coding part of ttRRF was amplified from these suppressor variants by PCR and subjected to DNA sequencing and complementation test.

Other DNA procedures

Single- or double-stranded DNAs were sequenced by means of dideoxynucleotide chain termination (Sanger et al., 1977). PCR proceeded according to standard methods (Saiki et al., 1988), and other DNA manipulations were conducted as described (Sambrook et al., 1989). The LB medium contained 1% Bacto-tryptone, 0.5% Yeast extract and 0.5% NaCl (Miller, 1972) and was supplemented with relevant antibiotics.

ACKNOWLEDGMENTS

We thank Drs. Don Court and Xinhua Ji for critical reading of the manuscript and valuable comments. This work was supported in part by grants from The Ministry of Education, Science, Sports and Culture, Japan (to Y.N.); the Human Frontier Science Program (awarded in 1993 and 1997 to Y.N.); the BRAIN Basic Research for Innovation Biosciences Program of Bio-oriented Technology Research Advancement Institution, Japan (to Y.N.); the Russian Academy of Sciences and the Russian Foundation for Basic Research (to M.G.); and the International Research Scholar's award from the Howard Hughes Medical Institute (to M.G.). T.T. and K.I. are BRAIN Research Fellows, and O.F.T. is a recipient of the cooperative research studentship from The Ministry of Education, Science, Sports and Culture, Japan.

Received May 30, 2000; returned for revision
July 11, 2000; revised manuscript received July 17, 2000

REFERENCES

Agrawal RK, Penczek P, Grassucci RA, Frank J. 1998. Visualization of the elongation factor G on the *Escherichia coli* 70S ribosome: The mechanism of translocation. *Proc Natl Acad Sci USA 95*: 6134–6138.

Brünger AT. 1992. *X-PLOR manual, version 3.1*. New Haven: Yale University Press.

Collaborative Computational Project, Number 4. 1994. The CCP4 suite: Programs for protein crystallography. *Acta Cryst D50*:760–763.

Crawford D-JG, Ito K, Nakamura Y, Tate WP. 1999. Indirect regulation of termination efficiency at highly expressed genes and recoding sites by the factor recycling function of *Escherichia coli* release factor RF3. *EMBO J 18*:727–732.

Freistroffer DV, Pavlov MY, MacDougall J, Buckingham RH, Ehrenberg M. 1997. Release factor RF3 in *E. coli* accelerates the dissociation of release factors RF1 and RF2 from the ribosome in a GTP-dependent manner. *EMBO J 16*:4126–4133.

Fujiwara T, Ito K, Nakayashiki T, Nakamura Y. 1999. Amber mutations in ribosome recycling factors of *Escherichia coli* and *Thermus thermophilus*: Evidence for C-terminal modulator element. *FEBS Lett 447*:297–302.

Hirashima A, Kaji A. 1972. Factor-dependent release of ribosomes from messenger RNA: Requirement for two heat-stable factors. *J Mol Biol 65*:43–58.

Ito K, Uno M, Nakamura Y. 1998. Single amino acid substitution in prokaryote polypeptide release factor 2 permits it to terminate translation at all three stop codons. *Proc Natl Acad Sci USA 95*:8165–8169.

Ito K, Uno M, Nakamura Y. 2000. A tripeptide "anticodon" deciphers stop codons in messenger RNA. *Nature 403*:680–684.

Janosi L, Hara H, Zhang S, Kaji A. 1996. Ribosome recycling by ribosome recycling factor (RRF): An important but overlooked step of protein biosynthesis. *Adv Biophys 32*:121–201.

Janosi L, Mottagui-Tabar S, Isaksson LA, Sekine Y, Ohtsubo E, Zhang S, Goon S, Nelken S, Shuda M, Kaji A. 1998. Evidence for in vivo ribosome recycling, the fourth step in protein biosynthesis. *EMBO J 17*:1141–1151.

Karimi R, Pavlov M, Buckingham R, Ehrenberg M. 1999. Novel roles for classical factors at the interface between translation termination and initiation. *Mol Cell 3*:601–609.

Laskowski RA, MacArthur MW, Moss DS, Thornton JM. 1993. PROCHECK: A program to check the stereochemical quality of protein structures. *J Appl Cryst 26*:283–291.

Luzzati P. 1952. Traitement statistique des erreurs dans dans la détermination des structures cristallines. *Acta Crystallogr 5*:802–810.

Kim KK, Min K, Suh SW. 2000. Crystal structure of the ribosome recycling factor from *Escherichia coli*. *EMBO J 19*:2362–2370.

Matsumoto A, Tomimoto M, Go N. 1999. Dynamical structure of transfer RNA studied by normal mode analysis. *Eur Biophys J 28*:369–379.

Miller J. 1972. *Experiments in molecular genetics*. Cold Spring Harbor, New York: Cold Spring Harbor Laboratory Press.

Nakamura Y, Ito K. 1998. How protein reads the stop codon and terminates translation. *Genes Cells 3*:265–278.

Nakamura Y, Ito K, Ehrenberg M. 2000. Mimicry grasps reality in translation termination. *Cell 101*:349–352.

Nakamura Y, Ito K, Isaksson LA. 1996. Emerging understanding of translation termination. *Cell 87*:147–150.

Nissen P, Kjeldgaard M, Nyborg J. 2000. Macromolecular mimicry. *EMBO J 19*:489–495.

Nissen P, Kjeldgaard M, Thirup S, Polekhina G, Reshetnikova L, Clark BFC, Nyborg J. 1995. Crystal structure of the ternary complex of Phe-tRNA^{Phe}, EF-Tu, and a GTP analog. *Science 270*: 1464–1472.

Oshima T, Ito K, Kabayama H, Nakamura Y. 1995. Regulation of *lrp* gene expression by H-NS and Lrp proteins in *Escherichia coli*: Dominant negative mutations in *lrp*. *Mol Gen Genet 247*:521–528.

Otwinowski Z, Minor W. 1997. Processing of X-ray diffraction data collected in oscillation mode. *Methods Enzymol 276*:307–326.

Pavlov MY, Freistroffer DV, MacDougall J, Buckingham RH, Ehrenberg M. 1997. Fast recycling of *Escherichia coli* ribosomes requires both ribosome recycling factor (RRF) and release factor RF3. *EMBO J 16*:4134–4141.

Poole ES, Brown CM, Tate WP. 1995. The identity of the base following the stop codon determines the efficiency of in vivo translational termination in *Escherichia coli*. *EMBO J 14*:151–158.

Rolland N, Janosi L, Block MA, Shuda M, Teyssier E, Miège C, Chénielet C, Carde J-P, Kaji A, Joyard J. 1999. Plant ribosome recycling factor homologue is a chloroplastic protein and is bactericidal in *Escherichia coli* carrying temperature-sensitive ribosome recycling factor. *Proc Natl Acad Sci USA 96*:5464–5469.

Ruff M, Krishnaswamy S, Boeglin M, Poterszman A, Mitschler A, Podjarny A, Rees B, Thierry JC, Moras D. 1991. Class II aminoacyl transfer RNA synthetases: Crystal structure of yeast aspartyl-tRNA synthetase complexed with tRNA^{Asp}. *Science 252*: 1682–1689.

Saiki RK, Gelfand DH, Stoffel S, Scharf SJ, Higuchi R, Horn GT, Mullis KB, Erlich HA. 1988. Primer-directed enzymatic amplification of DNA with a thermostable DNA polymerase. *Science 239*: 487–491.

Sambrook J, Fritsch EF, Maniatis T. 1989. *Molecular cloning: A laboratory manual*, 2nd ed. Cold Spring Harbor, New York: Cold Spring Harbor Laboratory Press.

Sanger F, Nicklen S, Coulson AR. 1977. DNA sequencing with chain-terminating inhibitors. *Proc Natl Acad Sci USA 74*:5463–5467.

Selmer M, Al-Karadaghi S, Hirokawa G, Kaji A, Liljas A. 1999. Crystal structure of *Thermotoga maritima* ribosome recycling factor: A tRNA mimic. *Science 286*:2349–2352.

Song H, Mugnier P, Das AK, Webb HM, Evans DR, Tuite MF, Hemmings BA, Barford D. 2000. The crystal structure of human eukaryotic release factor eRF1—mechanism of stop codon recognition and peptidyl-tRNA hydrolysis. *Cell 100*:311–321.

Wilson KS, Noller HF. 1998. Mapping the position of translational elongation factor EF-G in the ribosome by directed hydroxyl radical probing. *Cell 92*:131–139.

Yamamoto M, Kumasaka T, Fujisawa T, Ueki T. 1998. Trichromatic concept at SPring-8 RIKEN beamline I. *J Synchrotron Rad 5*: 222–226.

Yarus M, Curran J. 1992. The translational context effect. In: Hatfield DL, Lee BY, Pirtle RM, eds. *Transfer RNA in protein synthesis*. Boca Raton, Florida: CRC Press. pp 319–365.